RESEARCH

Check for updates

Highly sensitive near-infrared SERS nanoprobes for in vivo imaging using gold-assembled silica nanoparticles with controllable nanogaps

Sungje Bock[1†], Yun-Sik Choi[2†], Minhee Kim[1†], Yewon Yun[1], Xuan-Hung Pham[1], Jaehi Kim[1], Bomi Seong[1], Wooyeon Kim[1], Ahla Jo[1], Kyeong-Min Ham[1], Sung Gun Lee[2], Sang Hun Lee[3], Homan Kang[4], Hak Soo Choi[4], Dae Hong Jeong[2], Hyejin Chang[5*], Dong-Eun Kim[1*] and Bong-Hyun Jun[1*]

Abstract

Background: To take advantages, such as multiplex capacity, non-photobleaching property, and high sensitivity, of surface-enhanced Raman scattering (SERS)-based in vivo imaging, development of highly enhanced SERS nanoprobes in near-infrared (NIR) region is needed. A well-controlled morphology and biocompatibility are essential features of NIR SERS nanoprobes. Gold (Au)-assembled nanostructures with controllable nanogaps with highly enhanced SERS signals within multiple hotspots could be a breakthrough.

Results: Au-assembled silica (SiO_2) nanoparticles (NPs) (SiO_2@Au@Au NPs) as NIR SERS nanoprobes are synthesized using the seed-mediated growth method. SiO_2@Au@Au NPs using six different sizes of Au NPs (SiO_2@Au@Au$_{50}$–SiO_2@Au@Au$_{500}$) were prepared by controlling the concentration of Au precursor in the growth step. The nanogaps between Au NPs on the SiO_2 surface could be controlled from 4.16 to 0.98 nm by adjusting the concentration of Au precursor (hence increasing Au NP sizes), which resulted in the formation of effective SERS hotspots. SiO_2@Au@Au$_{500}$ NPs with a 0.98-nm gap showed a high SERS enhancement factor of approximately 3.8×10^6 under 785-nm photoexcitation. SiO_2@Au@Au$_{500}$ nanoprobes showed detectable in vivo SERS signals at a concentration of 16 µg/mL in animal tissue specimen at a depth of 7 mm. SiO_2@Au@Au$_{500}$ NPs with 14 different Raman label compounds exhibited distinct SERS signals upon subcutaneous injection into nude mice.

Conclusions: SiO_2@Au@Au NPs showed high potential for in vivo applications as multiplex nanoprobes with high SERS sensitivity in the NIR region.

Keywords: Surface-enhanced Raman spectroscopy (SERS), Gold nanoparticle, Nanogap, Hotspot, In vivo imaging

*Correspondence: hjchang@kangwon.ac.kr; kimde@konkuk.ac.kr; bjun@konkuk.ac.kr
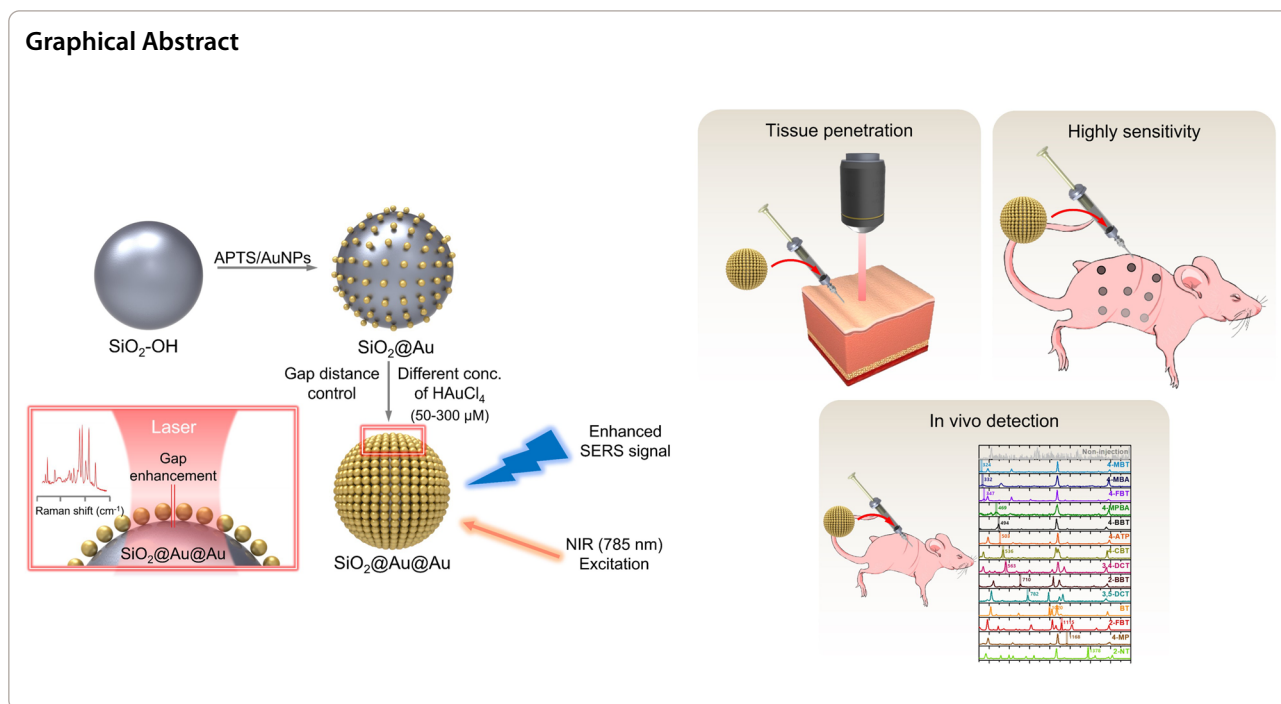†Sungje Bock, Yun-Sik Choi and Minhee Kim contributed equally to this work
[1] Department of Bioscience and Biotechnology, Konkuk University, Seoul 05029, South Korea
[5] Division of Science Education, Kangwon National University, Chuncheon 24341, South Korea
Full list of author information is available at the end of the article

Bock *et al. Journal of Nanobiotechnology*   (2022) 20:130

Page 2 of 12

Graphical Abstract

Background

In vivo imaging is a powerful tool for observing the localized effects of drugs as well as biological phenomena in living tissues or organs. However, conventional imaging methods, such as magnetic resonance imaging or molecular imaging based on fluorophores, usually lack multiplex capability [1–3]. Moreover, fluorescence imaging suffers from sensitivity issue owing to the autofluorescence of living animal tissues in the presence of visible light. To overcome these problems, in vivo imaging using near-infrared (NIR) light has attracted considerable attention owing to the good penetration ability of NIR radiation into tissues [4–6]. To observe effects of different drugs simultaneously and their multiple tumor-targeting abilities using in vivo imaging techniques, multiplexing capacity is one of the virtues for in vivo imaging probes [7]. However, widely used NIR imaging probes, such as fluorescent dyes and upconversion luminescent nanoparticles (NPs), still exhibit issues of spectral overlap, hindering multiplex imaging [8–10].

Surface-enhanced Raman scattering (SERS) is a powerful tool for biological and chemical analyses and imaging owing to its high sensitivity, multiplexing ability, and selectivity [11–19]. SERS using NIR-active NPs has been applied to multiplex imaging, given the narrow bandwidth (< 2 nm) of Raman signals [20–22]. Among several types of possible SERS NPs, gold NPs (Au NPs) have wide range of bioapplications [23–30] based on the plasmon resonance phenomenon with visible and NIR radiations

[31] because of their good biocompatibility and high stability under biological conditions compared to NPs of other metals (for example, silver and copper) [32–34]. However, compared with silver NPs (Ag NPs) that provide better SERS enhancement owing to their strong surface plasmon resonance properties [35], Au NPs still have relatively weak SERS signal enhancement ability.

Many researchers have attempted to build Au nanostructures to embed controllable nanogaps or to be effective as SERS nanoprobes, overcoming the limited SERS enhancement performance of Au NPs [36–38]. Wang et al. reported seed-mediated growth method for Au nanostars that exhibited strong absorbance in the NIR region and showed the possibility of imaging and treating cancer cells through photothermal therapy (PTT) [39]. Ding et al. reported sea urchin-like, flower-like, meatball-like, and polyhedral Au mesopores of various sizes and shapes [40]. Au NP-assembled nanostructures exhibited strong SERS signals, generating multiple hotspots within the nanogaps between small Au NPs [41]. However, Au NP-assembled nanostructures generated without seed-mediated growth method (usually with a long tedious synthesis process) were heterogenous in shape and had uncontrolled nanogaps.

We recently prepared Au-assembled silica (SiO_2) NPs by precisely controlling the size of Au NPs on the surface of SiO_2 NPs [42]. Currently, there are no studies on the relationship between nanogaps within Au NPs and their SERS characteristics, which can be a

Bock *et al. Journal of Nanobiotechnology*   (2022) 20:130

Page 3 of 12

critical feature for NIR SERS imaging. In this study, Au NP-assembled SiO$_2$ NPs (SiO$_2$@Au@Au NPs) with small nanogaps were synthesized to develop NIR-active SERS nanoprobes. Various types of nanogaps as SERS hotspots were generated by controlling the degree of Au NP growth on the surface of SiO$_2$ NPs. Our SiO$_2$@Au@Au NPs showed single-particle level detection sensitivity under 785-nm NIR laser photoexcitation and were applied for in vitro imaging using HCT 116 cell line. To evaluate them as potential SERS nanoprobes, SiO$_2$@Au@Au NPs labeled with 4-fluorobenzenethiol (4-FBT) were used to investigate the signal penetration depth in the porcine tissue and the detectable concentration limit upon subcutaneous injection. SiO$_2$@Au@Au NPs labeled with 14 types of Raman labeling compounds (RLCs) exhibited distinct Raman spectra and unique bands upon subcutaneous injection. The highly enhanced SERS signals and spectroscopic features of SiO$_2$@Au@Au NPs indicate that our NIR nanoprobes have the potential for use in multiplex imaging with various RLCs in vivo.

Materials and methods

Materials

Tetraethyl orthosilicate (TEOS), (3-aminopropyl)triethoxysilane (APTS), tetrakis(hydroxymethyl)-phosphonium chloride (THPC), polyvinylpyrrolidone (PVP), gold(III) chloride trihydrate (HAuCl$_4$), ascorbic acid (AA), paraformaldehyde, 4-FBT, 2-naphthalenethiol (2-NT), 3,5-dichlorobenzenethiol (3,5-DCT), 4-chlorobenzenethiol (4-CBT), 4-methylbenzenethiol (4-MBT), 4-mercaptophenol (4-MP), 4-bromobenzenethiol (4-BBT), 4-aminothiophenol (4-ATP), 4-mercaptobenzoic acid (4-MBA), 4-mercaptophenyl boronic acid (4-MPBA), benzenethiol (BT), 2-BBT, 3,4-DCT, and 2-FBT were purchased form Sigma-Aldrich (St. Louis, MO, USA). Ethanol (EtOH) and aqueous ammonium hydroxide (NH$_4$OH) were purchased from Daejung (Sihung-si, Gyeonggi-do, South Korea). Sodium hydroxide (NaOH) was purchased from Samchun (Pyeongtaek-si, Gyeonggi-do, South Korea). Deionized water (DW) was obtained using a Millipore water purification system (Vivagen, Seongnam-si, Gyeonggi-do, South Korea). HCT 116 cells were purchased from the American Type Culture Collection (ATCC) (Manassas, VA, USA). Roswell Park Memorial Institute (RPMI) 1640 medium was purchased from Biowest (Riverside, MO, USA). Fetal bovine serum (FBS) was purchased from JCBIO (Seoul, South Korea). Penicillin–streptomycin was purchased from Welgene (Gyeongsan-si, Gyeongsangbuk-do, South Korea). Phosphate-buffered saline (PBS) was purchased from BYLABS (Hanam-si, Gyeonggi-do, South Korea).

Sodium dodecyl sulfate (SDS) was purchased from LPS Solution (Daejeon-si, South Korea). Eight-week-old female BALB/c athymic nude mice were purchased from Orient Bio Inc. (Seongnam-si, Gyeonggi-do, Korea).

Raman spectroscopy measurements

All SERS spectra were obtained using a confocal micro Raman system (XperRF, Nanobase) equipped with an optical microscope (BX41M-LED; Olympus, Tokyo, Japan). The signal was detected using a thermoelectrically cooled (-60 °C) charge-coupled device detector (Idus 416, Andor Technology). The 532-, 660-, and 785-nm photoexcitation lasers were focused, and the Raman signals except the SERS enhancement factor (EF) calculation data were collected using a × 10 objective lens (0.25 NA, Olympus).

Preparation of SiO$_2$@Au@Au NPs

SiO$_2$@Au was synthesized using a previously reported method [42]. Au NPs (3 nm) were prepared using the Turkevich method. Briefly, 1.5 mL of 0.2 M NaOH, 12 μL of THPC, and 1.5 mL of HAuCl$_4$ solution (50 mM) were added to 47.5 mL of DW. The mixture was vigorously stirred for 1 h and stored in a refrigerator for at least two days. In addition, 62 μL of APTS and 40 μL of NH$_4$OH were added to 1 mL of SiO$_2$ NPs (50 mg/mL), and the mixture was stirred overnight at 700 rpm to produce aminated SiO$_2$ NPs (SiO$_2$-NH$_2$ NPs), which were then washed several times with EtOH by centrifugation; subsequently, 10 mL of Au NPs and 200 μL of SiO$_2$-NH$_2$ NPs (10 mg/mL) were mixed and stirred overnight. SiO$_2$@Au NPs were obtained after washing several times with EtOH by centrifugation, which were dispersed in 2 mL of DW containing 2 mg of PVP.

SiO$_2$@Au@Au NPs were prepared according to a method described in our previous study [42] with slight modifications. Briefly, SiO$_2$@Au@Au NPs were synthesized using the seed-mediated growth method with SiO$_2$@Au NP as a seed and Au precursor. To grow Au into SiO$_2$@Au seed, 200 μL of SiO$_2$@Au NPs (1 mg/mL) was dispersed in 9.8 mL DW containing 10 mg of PVP. This suspension was stirred after adding 20 μL of HAuCl$_4$ (10 mM) and treated with 40 μL of AA (10 mM) every 5 min until the desired concentration of Au^{3+} was achieved (50, 100, 200, 300, 400, and 500 μM), which was then washed several times with EtOH by centrifugation to obtain SiO$_2$@Au@Au$_{50}$–SiO$_2$@Au@Au$_{500}$ NPs.

Labeling SiO$_2$@Au@Au with Raman compounds

An RLC solution (2 mM) was prepared and added to 1 mL of SiO$_2$@Au@Au NPs (1 mg/mL). The mixture

Bock *et al. Journal of Nanobiotechnology* (2022) 20:130

Page 4 of 12

was vigorously shaken for 1 h at 25 ℃, and thus obtained RLC-conjugated SiO_2@Au@Au NPs were washed several times with EtOH by centrifugation. Subsequently, Raman-labeled SiO_2@Au@Au (SiO_2@Au@Au-RLC) NPs were redispersed in 1 mL of EtOH.

SERS measurement of SiO_2@Au@Au-RLC NPs
SiO_2@Au@Au-RLC suspension (1 mg/mL) was injected into a capillary tube. SERS spectrum of each NP was measured thrice using microscopic Raman system. Measurement was carried out under 532-nm photoexcitation at 1 mW, 660-nm photoexcitation at 1.2 mW, and 785-nm photoexcitation at 2.1 mW laser power using a ×10 objective lens with 5-s acquisition time.

Calculation of SERS enhancement factor (EF)
Further Raman spectroscopic studies and bioapplication experiments were carried out using SiO_2@Au@Au$_{500}$, where the SERS EF of SiO_2@Au@Au$_{500}$-4-FBT NPs under 785-nm photoexcitation was estimated using the following equation: $EF = (I_{SERS} \times N_{normal})/(I_{normal} \times N_{SERS})$, where I_{SERS} and I_{normal} indicate the intensity of the Raman band from SERS and normal Raman, respectively, and N_{normal} and N_{SERS} are the numbers of 4-FBT molecules in the pure and assembled forms, respectively, on the surface of SiO_2@Au@Au$_{500}$-4-FBT NPs. The Raman signal intensity was measured for both pure 4-FBT and single-particle level using identical ×100 objective lens (0.90 NA, Olympus) under the following conditions: 0.3 mW laser power and 5-s acquisition time. The 4-FBT peak at 1075 cm^{-1} was used to estimate the EF. I_{SERS} was defined as an average value of the peak intensities of 20 individual particles. The probing volume (18.84 μm^2) for the normal Raman measurement was approximated using a cylindrical form with a diameter of 2 μm and height of 6 μm. Assuming that 4-FBT molecules form a monolayer on the surface of NPs, N_{SERS} was calculated based on the surface area of NPs (assuming that SiO_2@Au@Au$_{500}$-4-FBT has a spherical shape, r = 115 nm) and the molecular footprint of 4-FBT (0.383 nm^2/molecule) [43].

Cytotoxicity of SiO_2@Au@Au$_{500}$-4-FBT in HCT 116 cells
HCT 116 cells (human colon cancer cell line) were cultured in RPMI 1640 medium supplemented with 10% heat-inactivated FBS and 1% penicillin/streptomycin at 37 ℃ in humidified air with 5% CO_2. Cytotoxicity of NPs was estimated using the crystal violet assay. Cells were seeded in 96-well plates and incubated with different concentrations (0, 1.95, 3.90, 7.81, 15.63, 31.25, and 62.50 mg/mL) of SiO_2@Au@Au$_{500}$-4-FBT NPs at 37 °C for 24 h. After incubation, the culture medium was removed, and the cells were fixed with 4% paraformaldehyde for 1 h. Then, the cells were washed with DW and air dried. The cells in each well were treated with 100 μL of 0.5% crystal violet solution. After 10 min, the solution was removed and the plates were washed with DW and air dried. Subsequently, the cells were lysed with 1% SDS, and absorbance was measured using VICTOR X3 multilabel plate reader (PerkinElmer, Waltham, MA, USA) at 570 nm.

SERS imaging of HCT 116 cells
Cells were seeded in a 60-mm dish and incubated with 50 μg/mL SiO_2@Au@Au$_{500}$-4-FBT NPs at 37 ℃ for 24 h. After incubation, the culture medium was removed, and the cells were washed thrice with 1 × PBS. Cells were then fixed with 4% paraformaldehyde for 1 h, washed with PBS, and dried at room temperature. Then, the SERS mapping images were obtained by point-by-point mapping (step size: 1 μm) using a ×100 objective lens with a 785-nm excitation source, 0.3-mW laser power, and 1-s acquisition time.

Depth profile evaluation of SiO_2@Au@Au SERS signal
To evaluate the depth profile of SiO_2@Au@Au SERS signal, NPs were injected into the porcine tissue, and the Raman spectra were measured. First, 15 μL of SiO_2@Au@Au$_{500}$-4-FBT (1 mg/mL) was dispersed in DW and injected into the porcine tissue with a 26-gauge syringe at different depths (1, 3, 5, 7, and 9 mm). SERS signals of NPs inside the tissue were measured immediately after injection using a ×10 objective lens with a 785-nm excitation source, 2.1-mW laser power, and 10-s acquisition time.

In vivo multiplexing SERS imaging
To conduct multiplexing SERS imaging in nude mice, 14 different types of RLCs (4-MBT, 4-MBA, 4-FBT, 4-MPBA, 4-BBT, 4-ATP, 4-CBT, 3,4-DCT, 2-BBT, 3,5-DCT, BT, 2-FBT, 4-MP, and 2-NT) were conjugated to SiO_2@Au@Au. After adaptation for one week, the mice were euthanized and subcutaneously injected with 15 μL of SiO_2@Au@Au$_{500}$-RLC. Diluted SiO_2@Au@Au$_{500}$-4-FBT (1000, 500, 250, 125, 63, 31, 16, 8, and 4 μg/mL) were injected into another mouse. Each measurement was performed using a ×10 objective lens with a 785-nm excitation source, 2.1-mW laser power, and 10-s acquisition time. Mice were maintained in accordance with the guidelines approved by the Institutional Animal Care and Use Committee (IACUC) of the Konkuk University.
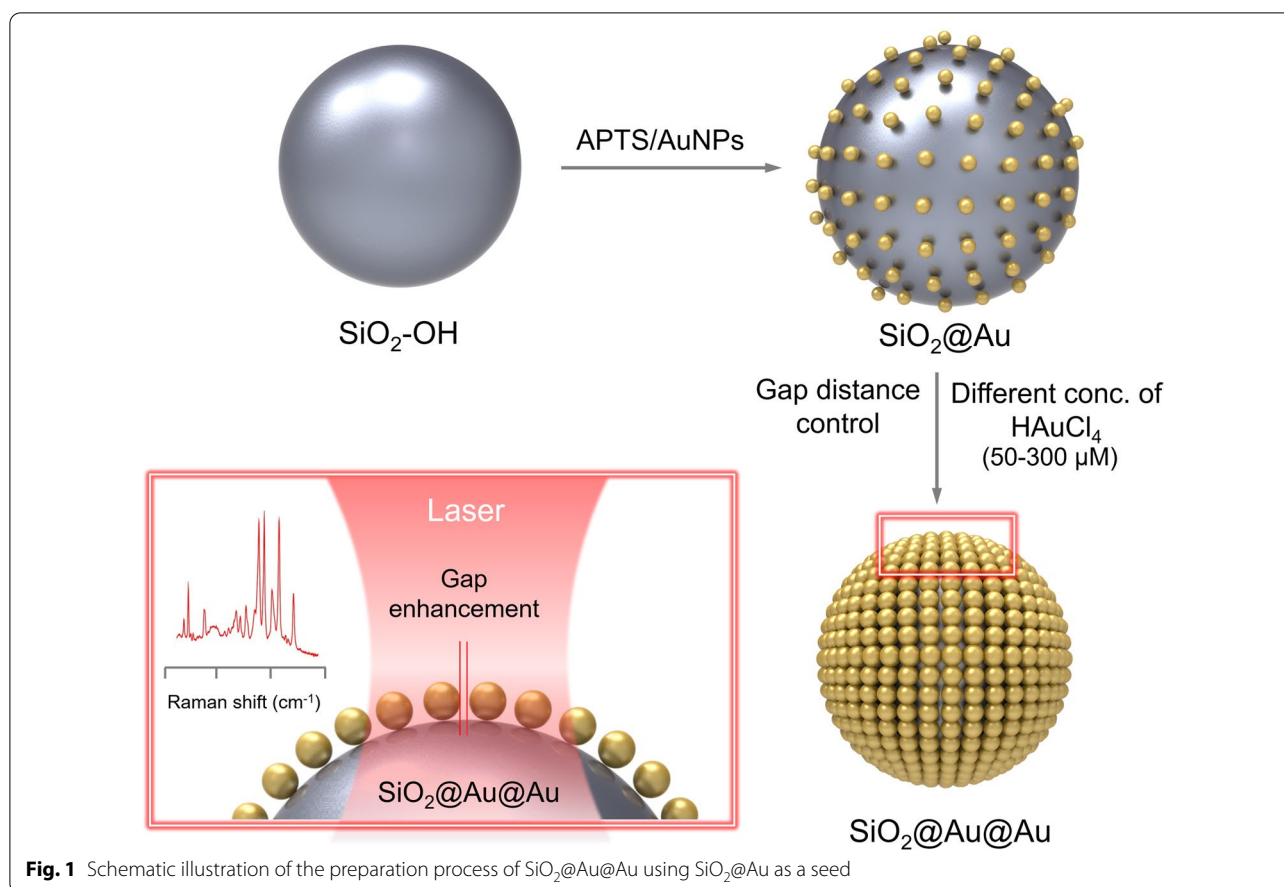
Bock *et al. Journal of Nanobiotechnology*   (2022) 20:130

Page 5 of 12

Fig. 1 Schematic illustration of the preparation process of SiO$_2$@Au@Au using SiO$_2$@Au as a seed
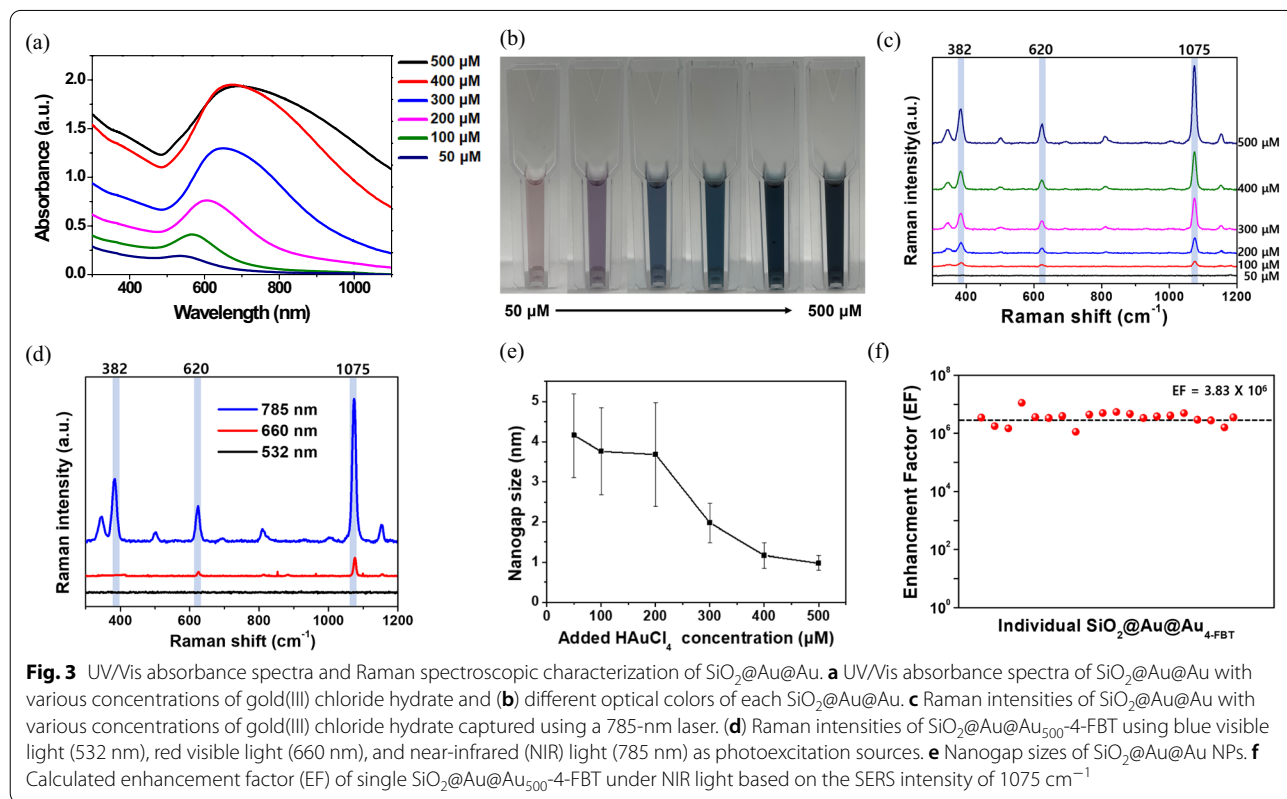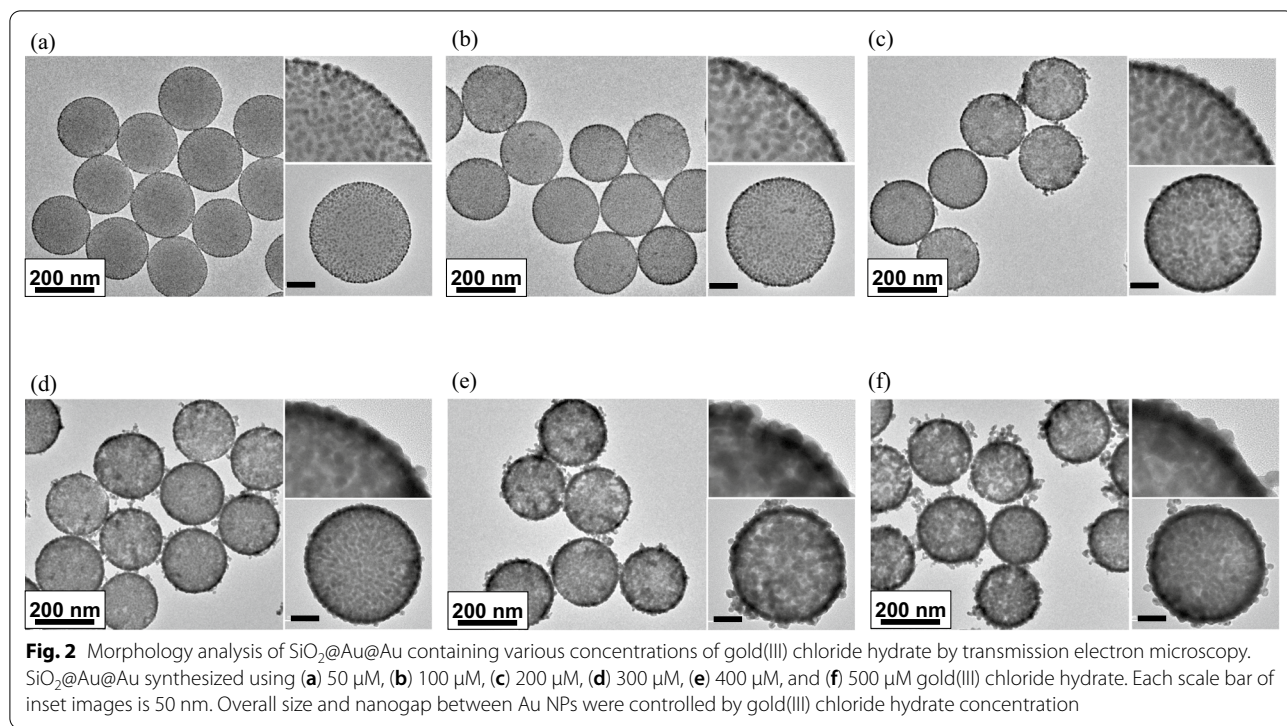
Results and discussion

Characterization and SERS properties of SiO$_2$@Au@Au NPs

SiO$_2$@Au@Au NPs were prepared using the method described in our previous study, with modifications [42]. Briefly, SiO$_2$@Au@Au was prepared by introducing Au NPs into SiO$_2$ to facilitate the growth of Au (Fig. 1). SiO$_2$ NPs were prepared according to the Stöber method (Additional file 1: Fig. S1). Subsequently, Au NPs were introduced into SiO$_2$ following treatment with APTS. SiO$_2$@Au was used as a seed in the seed-mediated growth method (Additional file 1: Fig. S2). SiO$_2$@Au seed (195.30 ± 13.16 nm) contained several Au NPs of very small size (3 nm) attached to the SiO$_2$ NP surface. It is imperative to control the size of Au NPs on the SiO$_2$ core to achieve a gap-enhanced SERS efficacy to create a strong local field between the Au NP gaps. In this regard, SiO$_2$@Au@Au NPs were fabricated using SiO$_2$@Au NP as a seed with varying concentrations of Au precursor (50, 100, 200, 300, 400, and 500 µM). After application of the growth method, the six prepared SiO$_2$@Au@Au NPs were 212.80 ± 7.35, 213.54 ± 7.14, 215.81 ± 8.30, 219.56 ± 9.36, 229.47 ± 9.85, and 229.48 ± 7.27 nm in size, corresponding to Au precursor concentrations of 50, 100, 200, 300, 400, and 500 µM, respectively (Fig. 2). With addition of higher concentration of Au precursor, the overall size of the NPs increased owing to the growth of Au NPs. The maximum concentration of Au precursor was 500 µM to prevent formation of merged structures (loss of particle morphology feature of Au NP) and seedings exclude Si NPs (Additional file 1: Fig. S3). The seed-mediated growth method allowed dense packing of Au NPs on the SiO$_2$ core surface, in contrast to the direct attachment of large-sized Au NPs on the SiO$_2$ core (Additional file 1: Fig. S4).

Figure 3a shows the absorbance of each prepared SiO$_2$@Au@Au NP. The absorbance increased at all wavelengths with increase in Au precursor concentration, particularly in the NIR region. In addition, the maximum absorption wavelength (λ_{max}) showed a red-shift with an increase in the concentration of Au precursor. This phenomenon is attributed to strong plasmonic coupling caused by the growth of Au NPs on the SiO$_2$ NP surfaces. As the absorbance changed, the color of the NPs dispersed in the solvent (EtOH) changed from light pink to dark blue (Fig. 3b).

Fig. 2 Morphology analysis of SiO$_2$@Au@Au containing various concentrations of gold(III) chloride hydrate by transmission electron microscopy. SiO$_2$@Au@Au synthesized using (**a**) 50 µM, (**b**) 100 µM, (**c**) 200 µM, (**d**) 300 µM, (**e**) 400 µM, and (**f**) 500 µM gold(III) chloride hydrate. Each scale bar of inset images is 50 nm. Overall size and nanogap between Au NPs were controlled by gold(III) chloride hydrate concentration

Fig. 3 UV/Vis absorbance spectra and Raman spectroscopic characterization of SiO$_2$@Au@Au. **a** UV/Vis absorbance spectra of SiO$_2$@Au@Au with various concentrations of gold(III) chloride hydrate and (**b**) different optical colors of each SiO$_2$@Au@Au. **c** Raman intensities of SiO$_2$@Au@Au with various concentrations of gold(III) chloride hydrate captured using a 785-nm laser. **d** Raman intensities of SiO$_2$@Au@Au$_{500}$-4-FBT using blue visible light (532 nm), red visible light (660 nm), and near-infrared (NIR) light (785 nm) as photoexcitation sources. **e** Nanogap sizes of SiO$_2$@Au@Au NPs. **f** Calculated enhancement factor (EF) of single SiO$_2$@Au@Au$_{500}$-4-FBT under NIR light based on the SERS intensity of 1075 cm^{-1}

Bock *et al. Journal of Nanobiotechnology*   (2022) 20:130

Page 7 of 12

To investigate the SERS characteristics of $SiO_2@Au@Au$, SERS spectra of the six $SiO_2@Au@Au$ NPs after treatment with 4-FBT were measured using three different laser lines (532, 660, and 785 nm) (Fig. 3c; Additional file 1: Fig. S4). Raman signals were not detectable for any of the six $SiO_2@Au@Au$-4-FBT NPs at 532 nm (Additional file 1: Fig. S4a). This was due to the relatively weak plasmonic resonances of the six $SiO_2@Au@Au$ NPs irradiated with light at a wavelength of 532 nm. SERS spectra obtained using a 660-nm laser revealed distinct bands for $SiO_2@Au@Au$ NPs treated with 200, 300, 400, and 500 µM Au precursor (Additional file 1: Fig. S4b). SERS signals measured using a 785-nm laser were stronger than those obtained using a 532-nm laser and 660-nm laser except the $SiO_2@Au@Au$ NPs treated with 50 µM Au precursor, for which no signal was detected (Fig. 3c; Additional file 1: Fig. S5). A comparison between 4-FBT SERS signal of $SiO_2@Au@Au_{500}$ at 1075 cm^{-1} peak showed that the Raman intensity with 785-nm photoexcitation was 7.7 times higher than that measured using 660-nm laser (Fig. 3d).

SERS spectra of $SiO_2@Au@Au$ NPs captured using 660-nm and 785-nm lasers showed enhanced Raman signals with an increase in the number of Au NPs on the SiO_2 surface. This could be attributed not only to the stronger absorbance but also to the narrower nanogap between Au NPs, leading to a highly amplified SERS signal. Transmission electron microscopy (TEM) images (Fig. 2) show that the nanogaps between Au NPs on the SiO_2 core gradually decreased as the concentration of Au NPs increased. The nanogap sizes were measured to be 4.16 ± 1.04, 3.76 ± 1.09, 3.68 ± 1.29, 1.98 ± 0.50, 1.17 ± 0.32, and 0.98 ± 0.19 nm for NPs treated with 50, 100, 200, 300, 400, and 500 µM Au precursor, respectively (Fig. 3e). The strongest Raman signal of $SiO_2@Au@Au$ NPs with 500 µM Au precursor during Au seed growth might be because the electromagnetic field was concentrated in 1-nm nanogaps. The seed-mediated growth method for $SiO_2@Au@Au$ NPs was validated as a powerful strategy to precisely control the nanogap size and maximize the SERS enhancement.

Considering that $SiO_2@Au@Au_{500}$ NPs have a higher absorbance in the NIR region and show the strongest Raman enhancement ability among all prepared NPs, the following experiments were performed using $SiO_2@Au@Au_{500}$. Using 4-FBT molecule as an RLC, the SERS spectra of 20 single particles of $SiO_2@Au@Au_{500}$-4-FBT were measured, and the average EF value was estimated to be 3.8×10^6 with good uniformity (3.45% relative standard deviation on log scale) (Fig. 3f). Compared to other noble metal-based NPs, the assembled

Table 1 Comparison of enhancement factor of different metal-assembled nanoparticles
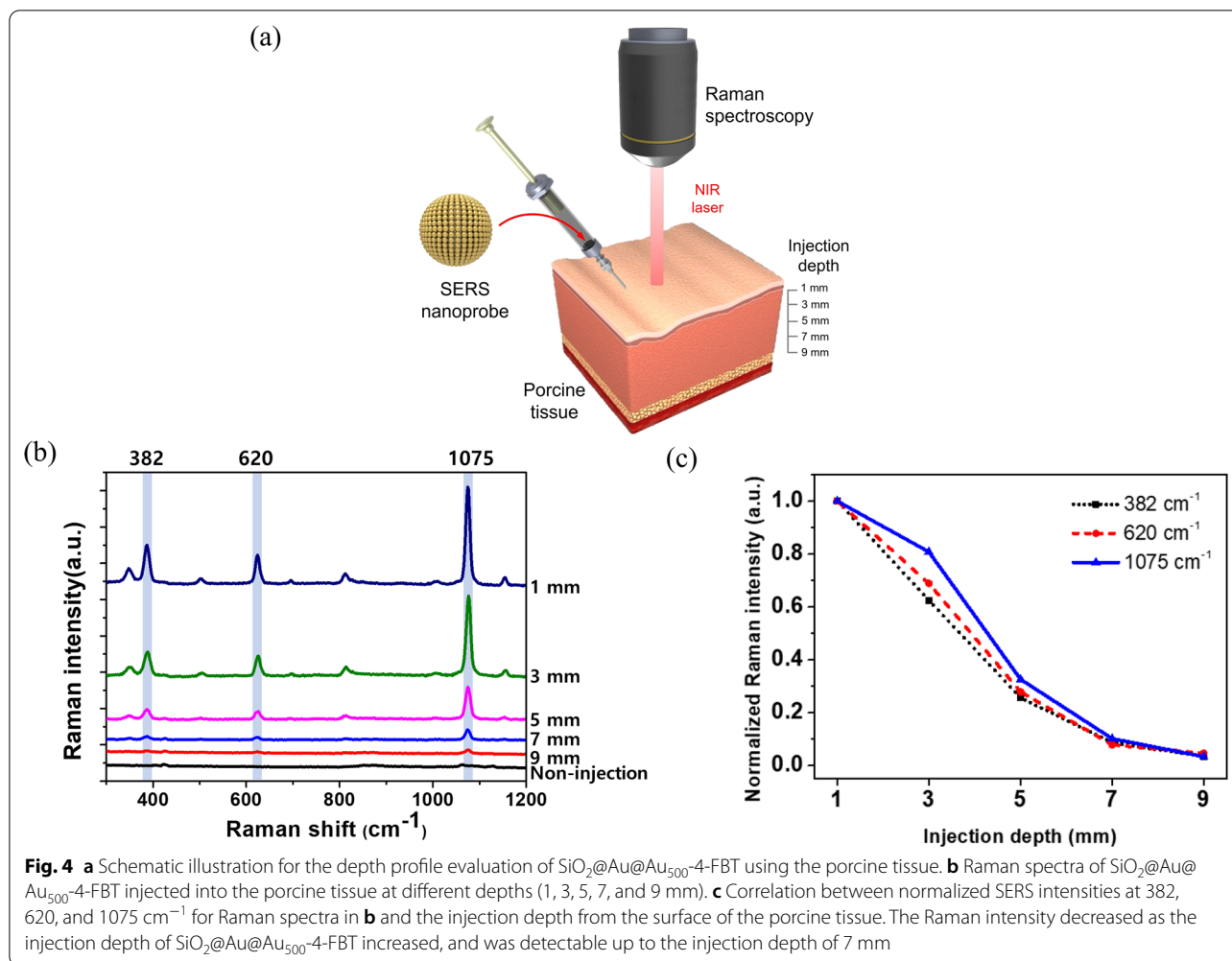
Composition	Nanoparticle (NP)	Enhancement factor (EF)	References
Silver (Ag)	Silica-encapsulated Ag-SiO_2 NP	1×10^5	[47]
	Bumpy silver nanoshell	2.2×10^7	[45]
Gold (Au)	Au/Ag hollow shell-assembled silica nanosphere	2.8×10^5	[48]
	Au-assembled silica NP	3.8×10^6	Current study

structure had a lower EF value owing to the large surface area for RLC binding. However, the higher intensity and signal uniformity of each nanocomposite could be an advantageous feature of the assembled structures [44]. $SiO_2@Au@Au_{500}$ exhibited higher EF values than those reported for other noble metal-assembled NPs (Table 1). Although the EF value is smaller than that of bumpy silver nanoshells, Au-assembled SiO_2 NPs are more stable than Ag-based NPs under biological conditions [45].

SERS imaging of HCT 116 cancer cell with $SiO_2@Au@Au_{500}$-4-FBT

Before using $SiO_2@Au@Au$ for in vitro applications, a cytotoxicity test was conducted using HCT 116 cell line. $SiO_2@Au@Au_{500}$-4-FBT NPs were prepared at a concentration of 62.5 µg/mL (26.38×10^8 particles/mL) and serially diluted for the cytotoxicity test (Additional file 1: Fig. S6). Cell viability was more than 90% at all concentrations of $SiO_2@Au@Au$ NPs within 24 h. Moreover, biocompatibility of $SiO_2@Au@Au_{500}$-4-FBT NPs at a concentration of 62.5 µg/mL or lower was confirmed.
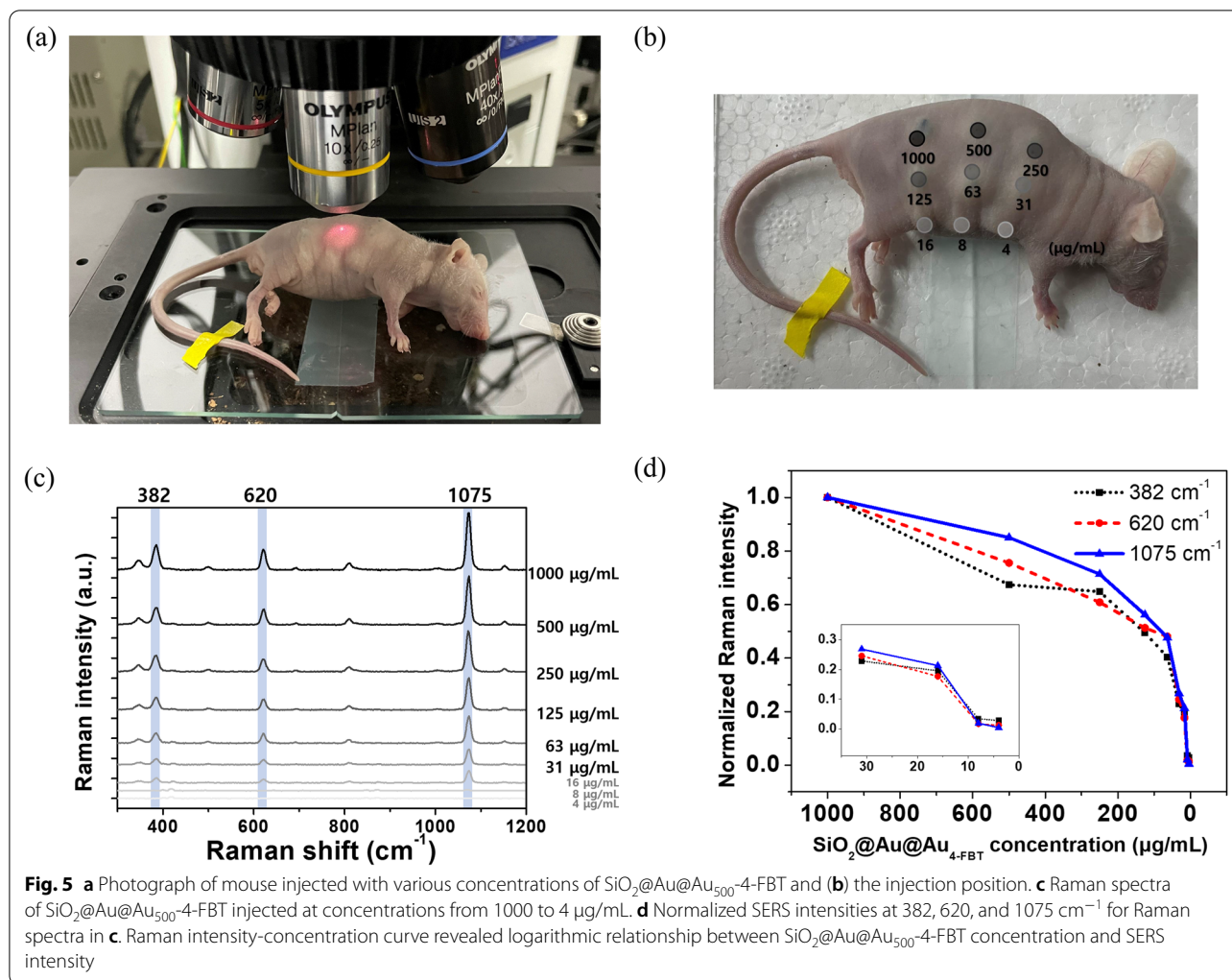
To obtain images of HCT 116 cancer cells through SERS, the cells were incubated with $SiO_2@Au@Au_{500}$-4-FBT NPs for 24 h. NPs were either attached to the cell surface or entered the cell, whereas the remaining NPs were washed out. Additional file 1: Figure S7a shows the SERS mapping image at 1075 cm^{-1}. The overlay image of HCT 116 cells and the adsorbed NPs showed that $SiO_2@Au@Au_{500}$-4-FBT NPs were attached to the edge of the cell. We compared the Raman intensity at different locations on the cell and observed no Raman signal outside the cell (i), weak Raman signal at the cell surface (ii), and extremely strong Raman signal inside the cell (iii) (Additional file 1: Fig. S7b). This observation confirmed the possibility of SERS imaging of cancer cells using $SiO_2@Au@Au$ NPs.

Bock *et al. Journal of Nanobiotechnology* (2022) 20:130

Page 8 of 12

Fig. 4 **a** Schematic illustration for the depth profile evaluation of $SiO_2@Au@Au_{500}$-4-FBT using the porcine tissue. **b** Raman spectra of $SiO_2@Au@Au_{500}$-4-FBT injected into the porcine tissue at different depths (1, 3, 5, 7, and 9 mm). **c** Correlation between normalized SERS intensities at 382, 620, and 1075 cm^{-1} for Raman spectra in **b** and the injection depth from the surface of the porcine tissue. The Raman intensity decreased as the injection depth of $SiO_2@Au@Au_{500}$-4-FBT increased, and was detectable up to the injection depth of 7 mm

Sensitivity of SERS signal of $SiO_2@Au@Au_{500}$-4-FBT

To investigate the SERS signal depth profile of $SiO_2@$ Au@Au, we injected $SiO_2@Au@Au_{500}$-4-FBT NPs into the porcine tissue at different depths (1, 3, 5, 7, and 9 mm) and measured the SERS spectra (Fig. 4a). As the depth increased, the Raman intensity decreased (Fig. 4b). However, a measurable signal was detected up to a depth of 7 mm. For an accurate analysis, the Raman band intensities at 382, 620, and 1075 cm^{-1} were normalized to the signal intensity at a depth of 1 mm (Fig. 4c). The Raman intensity decreased as NPs were injected deeper inside the porcine tissue, and the Raman spectra distinct from that of the tissue without NP injection was observed until a depth of 7 mm. We conclude that the $SiO_2@Au@Au$ NPs generated a detectable SERS signal until the maximum depth of 7 mm in animal tissues. Thus, SERS detection using $SiO_2@Au@Au$ NPs was attempted through subcutaneous injection into animals.

For in vivo imaging, it is crucial to use small amounts of NPs to avoid side effects such as blood clots [46]. To determine the detectable concentration limit, various concentrations of $SiO_2@Au@Au_{500}$-4-FBT from 1000 to 4 µg/mL were subcutaneously injected into nude mice, and the SERS spectra were measured using a 785-nm laser (Fig. 5a, b). The Raman intensity decreased as the concentration of $SiO_2@Au@Au_{500}$-4-FBT NPs decreased; however, a sufficient signal was observed at a concentration of 16 µg/mL (Fig. 5c). To compare these results, the Raman bands intensities at 382, 620, and 1075 cm^{-1} were normalized to the Raman signal at 1000 µg/mL (Fig. 5d). The strong SERS signal of $SiO_2@Au@Au_{500}$-4-FBT allowed for the subcutaneous detection of particles even at a very low concentration (16 µg/mL), showing sufficient signal sensitivity.

Bock *et al. Journal of Nanobiotechnology*   (2022) 20:130

Page 9 of 12

Fig. 5 **a** Photograph of mouse injected with various concentrations of SiO$_2$@Au@Au$_{500}$-4-FBT and (**b**) the injection position. **c** Raman spectra of SiO$_2$@Au@Au$_{500}$-4-FBT injected at concentrations from 1000 to 4 μg/mL. **d** Normalized SERS intensities at 382, 620, and 1075 cm^{-1} for Raman spectra in **c**. Raman intensity-concentration curve revealed logarithmic relationship between SiO$_2$@Au@Au$_{500}$-4-FBT concentration and SERS intensity

In vivo multiplex imaging potential

To investigate the multiplex imaging potential of SiO$_2$@Au@Au, 14 different RLC-treated NPs (SiO$_2$@Au@Au-RLC) were prepared and injected subcutaneously into nude mice (Fig. 6a). The Raman spectra from each location were measured using a 785-nm laser. Distinct Raman spectra were obtained for the 14 types of NPs (Fig. 6b), which showed unique bands for code (label) identification (4-MBT: 324 cm^{-1}; 4-MBA: 332 cm^{-1}; 4-FBT: 347 cm^{-1}; 4-MPBA: 469 cm^{-1}; 4-BBT: 494 cm^{-1}; 4-ATP: 503 cm^{-1}; 4-CBT: 536 cm^{-1}; 3,4-DCT: 563 cm^{-1}; 2-BBT: 710 cm^{-1}; 3,5-DCT: 782 cm^{-1}; BT: 1020 cm^{-1}; 2-FBT: 1115 cm^{-1}; 4-MP: 1168 cm^{-1}; and 2-NT: 1378 cm^{-1}). To the best of our knowledge, the present study used the highest number of labels for NIR-active nanoprobes; the previously reported maximum number of RLCs for multiplex imaging based on SERS was 10 [3]. Thus, our SiO$_2$@Au@Au NPs with multiple hotspots and narrow

nanogaps exhibited high stability, allowing attachment of 14 different RLCs.

Conclusions

SiO$_2$@Au@Au NPs were prepared using the seed-mediated growth method; six SiO$_2$@Au@Au NPs of different sizes were fabricated on the surface of SiO$_2$ NPs by controlling the concentration of Au precursor (50, 100, 200, 300, 400, and 500 μM). With increase in concentration of Au precursor, SiO$_2$@Au@Au showed stronger absorbance, particularly in the NIR region. In addition, multiple hotspots and narrow nanogaps of approximately 1 nm were obtained by increasing the concentration of Au precursor during the growth process, enabling single particle-level detection. The SERS measurement revealed the Raman signal of high intensity after 785-nm laser photoexcitation. SiO$_2$@Au@Au NPs obtained using 500 μM Au precursor exhibited an average SERS EF value of 3.83×10^6. SiO$_2$@Au@Au NPs

Bock *et al. Journal of Nanobiotechnology*   (2022) 20:130

Page 10 of 12

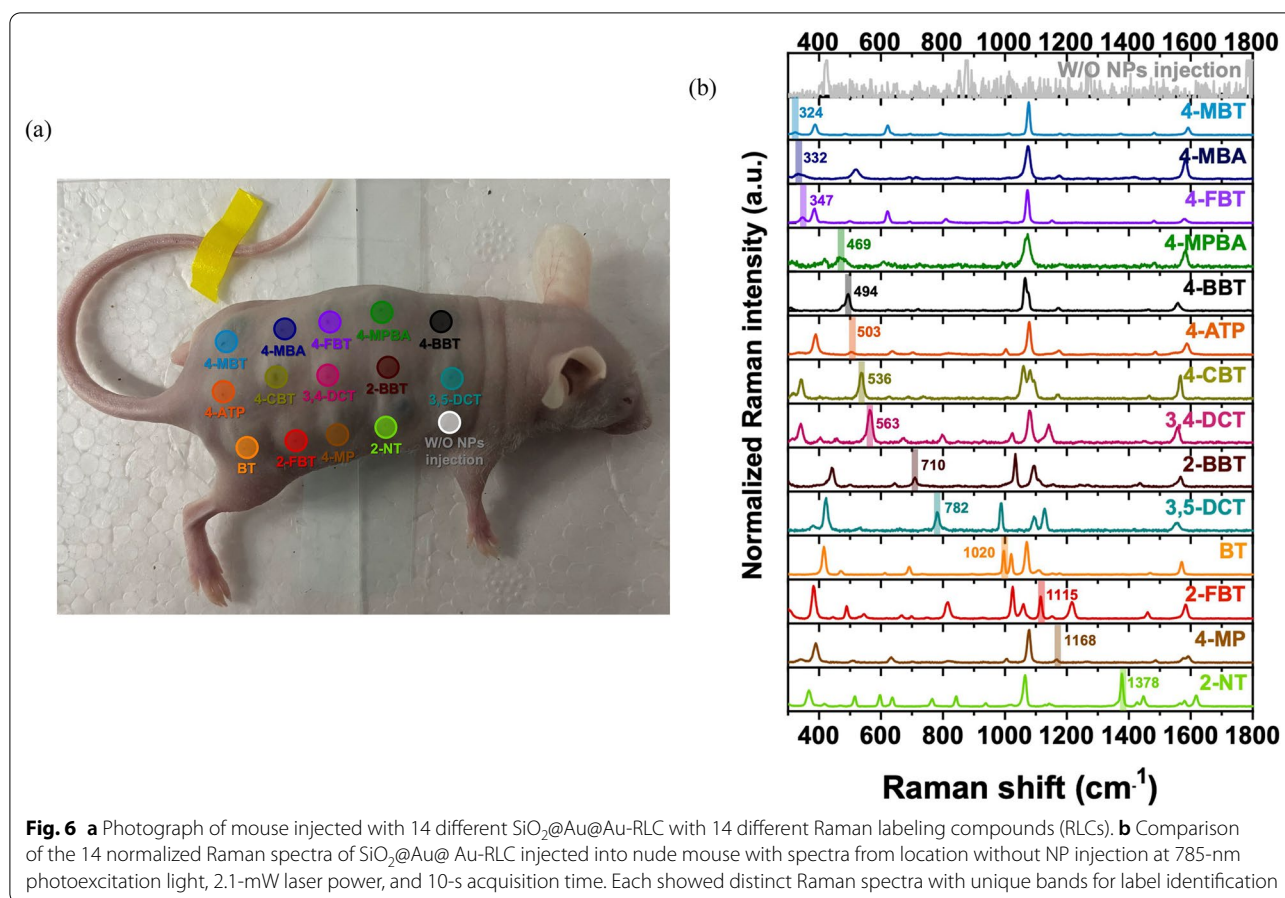**Fig. 6** **a** Photograph of mouse injected with 14 different SiO$_2$@Au@Au-RLC with 14 different Raman labeling compounds (RLCs). **b** Comparison of the 14 normalized Raman spectra of SiO$_2$@Au@ Au-RLC injected into nude mouse with spectra from location without NP injection at 785-nm photoexcitation light, 2.1-mW laser power, and 10-s acquisition time. Each showed distinct Raman spectra with unique bands for label identification

were successfully applied for the SERS imaging of HCT 116 cancer cells. In addition, owing to the advantages of NIR radiation and detection, the SERS signal could be measured even at a depth of 7 mm in the porcine tissue. The detectable concentration limit of NPs for subcutaneous injection was 16 µg/mL. Moreover, the multiplexing capability of the prepared SiO$_2$@Au@Au was investigated by subcutaneously injecting 14 different SiO$_2$@Au@Au-RLC NPs into nude mice. In this study, we fabricated highly sensitive NIR SERS nanoprobes with very strong SERS signals owing to their structure with uniformly synthesized multiple hotspots and narrow nanogaps. Along with the advantageous features of absorbing long-wavelength light and highly enhanced Raman signals, our SiO$_2$@Au@Au structure can potentially be used for multiplex molecular imaging and in vivo applications.

Abbreviations

AA: Ascorbic acid; APTS: (3-Aminopropyl)triethoxysilane; ATCC: American Type Culture Collection; BT: Benzenethiol; DW: Deionized water; EtOH: Ethanol; FBS: Fetal bovine serum; HAuCl$_4$: Gold(III) chloride trihydrate; NaOH: Sodium hydroxide; NH$_4$OH: Aqueous ammonium hydroxide; NIR: Near-infrared; NPs: Nanoparticles; PBS: Phosphate-buffered saline; PTT: Photothermal therapy; PVP: Polyvinylpyrrolidone; RLCs: Raman labeling compounds; SERS: Surface-enhanced Raman spectroscopy; SDS: Sodium dodecyl sulphate; SiO$_2$: Silica; SiO$_2$@Au@Au: Au-assembled silica nanoparticle; TEOS: Tetraethyl orthosilicate; THPC: Tetrakis(hydroxymethyl)-phosphonium chloride; 2-BBT: 2-Bromobenzenethiol; 2-FBT: 2- Fluorobenzenethiol; 2-NT: 2-Naphthalenethiol; 3,4-DCT: 3,4-Dichlorobenzenethiol; 3,5-DCT: 3,5-Dichlorobenzenethiol; 4-ATP: 4-Aminothiophenol; 4-BBT: 4-Bromobenzenethiol; 4-CBT: 4-Chlorobenzenethiol; 4-FBT: 4-Fluorobenzenethiol; 4-MBA: 4-Mercaptobenzoic acid; 4-MBT: 4-Methylbenzenethiol; 4-MP: 4-Mercaptophenol; 4-MPBA: 4-Mercaptophenyl boronic acid.

Supplementary Information

The online version contains supplementary material available at https://doi.org/10.1186/s12951-022-01327-7.

 Additional file 1: Fig S1. TEM image of SiO$_2$ NPs. **Fig S2.** TEM image of SiO$_2$@Au used as a seed. **Fig S3.** TEM image of SiO$_2$@Au@Au synthesized using 600 µM gold(III) chloride hydrate. **Fig S4.** TEM image of SiO$_2$@Au synthesized by directly attaching large-sized Au NPs (10–15 nm) to aminated silica (not a growth method). **Fig S5.** SERS intensities of SiO$_2$@Au@ Au-4-FBT synthesized using various concentrations of gold(III) chloride hydrate determined at (a) blue visible light (wavelength, 532 nm) and (b) red visible light (wavelength, 660 nm). **Fig S6.** Cytotoxicity test using HCT 116 cells incubated with different concentrations of SiO$_2$@Au@Au$_{500}$-4-FBT. **Fig S7.** (a) Optical image, SERS mapping image, and overlay image of human colon carcinoma (HCT 116) cells incubated with 50 µg/mL SiO$_2$@ Au@Au$_{500}$-4-FBT. (b) Raman intensities at different locations: outside the cell (i), on the cell surface (ii), and inside the cell (iii), corresponding to the overlay images shown in (a).

Bock *et al. Journal of Nanobiotechnology*   (2022) 20:130

Page 11 of 12

Declarations

Ethics approval and consent to participate
Not applicable.

Consent for publication
Not applicable.

Competing interests
The authors declare that they have no competing interests.

Author details
[1]Department of Bioscience and Biotechnology, Konkuk University, Seoul 05029, South Korea. [2]Department of Chemistry Education, Seoul National University, Seoul 08826, South Korea. [3]Department of Chemical and Biological Engineering, Hanbat National University, Deajeon 34158, South Korea. [4]Department of Radiology, Gordon Center for Medical Imaging, Massachusetts General Hospital and Harvard Medical School, Boston, MA 02114, USA. [5]Division of Science Education, Kangwon National University, Chuncheon 24341, South Korea.

References
1. Darvishi V, Navidbakhsh M, Amanpour S. Heat and mass transfer in the hyperthermia cancer treatment by magnetic nanoparticles. Heat Mass Transf. 2021. https://doi.org/10.1007/s00231-021-03161-3.
2. Gu Q, Joglekar T, Bieberich C, Ma R, Zhu L. Nanoparticle redistribution in PC3 tumors induced by local heating in magnetic nanoparticle hyperthermia: in vivo experimental study. J Heat Transfer. 2019;141(3):032402.
3. Zavaleta CL, Smith BR, Walton I, Doering W, Davis G, Shojaei B, Natan MJ, Gambhir SS. Multiplexed imaging of surface enhanced Raman scattering nanotags in living mice using noninvasive Raman spectroscopy. Proc Natl Acad Sci USA. 2009;106:13511–6.
4. Weissleder R. A clearer vision for in vivo imaging. Nat Biotechnol. 2001;19:316–7.
5. Yuan L, Lin W, Zhao S, Gao W, Chen B, He L, Zhu S. A unique approach to development of near-infrared fluorescent sensors for in vivo imaging. J Am Chem Soc. 2012;134:13510–23.
6. Kim JS, Kim Y-H, Kim JH, Kang KW, Tae EL, Youn H, Kim D, Kim S-K, Kwon J-T, Cho M-H. Development and in vivo imaging of a PET/MRI nanoprobe with enhanced NIR fluorescence by dye encapsulation. Nanomedicine. 2012;7:219–29.
7. Fan Y, Wang P, Lu Y, Wang R, Zhou L, Zheng X, Li X, Piper JA, Zhang F. Lifetime-engineered NIR-II nanoparticles unlock multiplexed in vivo imaging. Nat nanotechnol. 2018;13:941–6.
8. Haraguchi T, Shimi T, Koujin T, Hashiguchi N, Hiraoka Y. Spectral imaging fluorescence microscopy. Genes Cells. 2002;7:881–7.
9. Koide Y, Urano Y, Hanaoka K, Piao W, Kusakabe M, Saito N, Terai T, Okabe T, Nagano T. Development of NIR fluorescent dyes based on Si–rhodamine for in vivo imaging. J Am Chem Soc. 2012;134:5029–31.
10. Zhou J, Sun Y, Du X, Xiong L, Hu H, Li F. Dual-modality in vivo imaging using rare-earth nanocrystals with near-infrared to near-infrared (NIR-to-NIR) upconversion luminescence and magnetic resonance properties. Biomaterials. 2010;31:3287–95.
11. Schlücker S. Surface-enhanced Raman spectroscopy: concepts and chemical applications. Angew Chem Int Ed. 2014;53:4756–95.
12. Sharma B, Frontiera RR, Henry A-I, Ringe E, Van Duyne RP. SERS: materials, applications, and the future. Mater Today. 2012;15:16–25.
13. Lim D-K, Jeon K-S, Kim HM, Nam J-M, Suh YD. Nanogap-engineerable Raman-active nanodumbbells for single-molecule detection. Nat Mater. 2010;9:60–7.
14. Kneipp J, Kneipp H, Kneipp K. SERS—a single-molecule and nanoscale tool for bioanalytics. Chem Soc Rev. 2008;37:1052–60.
15. Hahm E, Kim Y-H, Pham X-H, Jun B-H. Highly reproducible surface-enhanced Raman scattering detection of alternariol using silver-embedded silica nanoparticles. Sensors. 2020;20:3523.
16. Pham X-H, Hahm E, Huynh K-H, Kim H-M, Son BS, Jeong DH, Jun B-H. Sensitive and selective detection of 4-aminophenol in the presence of acetaminophen using gold–silver core–shell nanoparticles embedded in silica nanostructures. J Ind Eng Chem. 2020;83:208–13.
17. Kang H, Koh Y, Jeong S, Jeong C, Cha MG, Oh M-H, Yang J-K, Lee H, Jeong DH, Jun B-H. Graphical and SERS dual-modal identifier for encoding OBOC library. Sens Actuators B Chem. 2020;303:127211.
18. Pham X-H, Hahm E, Kang E, Son BS, Ha Y, Kim H-M, Jeong DH, Jun B-H. Control of silver coating on Raman label incorporated gold nanoparticles assembled silica nanoparticles. Int J Mol Sci. 2019;20:1258.
19. Pham X-H, Hahm E, Kim TH, Kim H-M, Lee SH, Lee SC, Kang H, Lee H-Y, Jeong DH, Choi HS. Enzyme-amplified SERS immunoassay with Ag–Au bimetallic SERS hot spots. Nano Res. 2020;13:3338–46.
20. Keren S, Zavaleta C, Cheng ZD, de la Zerda A, Gheysens O, Gambhir S. Noninvasive molecular imaging of small living subjects using Raman spectroscopy. Proc Natl Acad Sci USA. 2008;105:5844–9.
21. Chang H, Kang H, Yang J-K, Jo A, Lee H-Y, Lee Y-S, Jeong DH. Ag Shell–Au satellite hetero-nanostructure for ultra-sensitive, reproducible, and homogeneous NIR SERS activity. ACS Appl Mater Interfaces. 2014;6:11859–63.
22. Nolan JP, Duggan E, Liu E, Condello D, Dave I, Stoner SA. Single cell analysis using surface enhanced Raman scattering (SERS) tags. Methods. 2012;57:272–9.
23. Jin Y. Engineering plasmonic gold nanostructures and metamaterials for biosensing and nanomedicine. Adv Mater. 2012;24:5153–65.
24. Han J, Zhang J, Yang M, Cui D, Jesus M. Glucose-functionalized Au nanoprisms for optoacoustic imaging and near-infrared photothermal therapy. Nanoscale. 2015;8:492–9.
25. Du L, Suo S, Wang G, Jia H, Liu KJ, Zhao B, Liu Y. Mechanism and cellular kinetic studies of the enhancement of antioxidant activity by using surface-functionalized gold nanoparticles. Chem Eur J. 2013;19:1281–7.
26. Zeng S, Yong K-T, Roy I, Dinh X-Q, Yu X, Luan F. A review on functionalized gold nanoparticles for biosensing applications. Plasmonics. 2011;6:491–506.
27. Frederix F, Friedt J-M, Choi K-H, Laureyn W, Campitelli A, Mondelaers D, Maes G, Borghs G. Biosensing based on light absorption of nanoscaled gold and silver particles. Anal Chem. 2003;75:6894–900.
28. Zhao W, Brook MA, Li Y. Design of gold nanoparticle-based colorimetric biosensing assays. ChemBioChem. 2008;9:2363–71.
29. Murphy CJ, Gole AM, Stone JW, Sisco PN, Alkilany AM, Goldsmith EC, Baxter SC. Gold nanoparticles in biology: beyond toxicity to cellular imaging. Acc Chem Res. 2008;41:1721–30.
30. Huang X, Jain PK, El-Sayed IH, El-Sayed MA. Plasmonic photothermal therapy (PPTT) using gold nanoparticles. Lasers Med Sci. 2008;23:217–28.
31. Anker JN, Hall WP, Lyandres O, Shah NC, Zhao J, Van Duyne RP. Biosensing with plasmonic nanosensors. J Nanosci Nanotechnol. 2010;308–319.
32. Lewinski N, Colvin V, Drezek R. Cytotoxicity of nanoparticles. Small. 2008;4:26–49.
33. Connor EE, Mwamuka J, Gole A, Murphy CJ, Wyatt MD. Gold nanoparticles are taken up by human cells but do not cause acute cytotoxicity. Small. 2005;1:325–7.

Bock *et al. Journal of Nanobiotechnology*   (2022) 20:130

Page 12 of 12

34. Giljohann DA, Seferos DS, Daniel WL, Massich MD, Patel PC, Mirkin CA. Gold nanoparticles for biology and medicine. Angew Chem Int. 2010;49:3280–94.
35. Lai C-H, Wang G-A, Ling T-K, Wang T-J, Chiu P-K, Chau Y-FC, Huang C-C, Chiang H-P. Near infrared surface-enhanced Raman scattering based on star-shaped gold/silver nanoparticles and hyperbolic metamaterial. Sci Rep. 2017;7:1–8.
36. Huang J, Zhang L, Chen B, Ji N, Chen F, Zhang Y, Zhang Z. Nanocomposites of size-controlled gold nanoparticles and graphene oxide: formation and applications in SERS and catalysis. Nanoscale. 2010;2:2733–8.
37. Ando J, Fujita K, Smith NI, Kawata S. Dynamic SERS imaging of cellular transport pathways with endocytosed gold nanoparticles. Nano Lett. 2011;11:5344–8.
38. Polavarapu L, Xu Q-H. Water-soluble conjugated polymer-induced self-assembly of gold nanoparticles and its application to SERS. Langmuir. 2008;24:10608–11.
39. Song C, Li F, Guo X, Chen W, Dong C, Zhang J, Zhang J, Wang L. Gold nanostars for cancer cell-targeted SERS-imaging and NIR light-triggered plasmonic photothermal therapy (PPTT) in the first and second biological windows. J Mater Chem B. 2019;7:2001–8.
40. You H, Ji Y, Wang L, Yang S, Yang Z, Fang J, Song X, Ding B. Interface synthesis of gold mesocrystals with highly roughened surfaces for surface-enhanced Raman spectroscopy. J Mater Chem. 2012;22:1998–2006.
41. Pazos-Perez N, Fitzgerald JM, Giannini V, Guerrini L, Alvarez-Puebla RA. Modular assembly of plasmonic core–satellite structures as highly brilliant SERS-encoded nanoparticles. Nanoscale Adv. 2019;1:122–31.
42. Seong B, Bock S, Hahm E, Huynh K-H, Kim J, Lee SH, Pham X-H, Jun B-H. Synthesis of densely immobilized gold-assembled silica nanostructures. Int J Mol Sci. 2021;22:2543.
43. Jiang P, Deng K, Fichou D, Xie S-S, Nion A, Wang C. STM imaging ortho- and para-fluorothiophenol self-assembled monolayers on Au (111). Langmuir. 2009;25:5012–7.
44. Jeon MJ, Ma X, Lee JU, Roh H, Bagot CC, Park W, Sim SJ. Precisely controlled three-dimensional gold nanoparticle assembly based on spherical bacteriophage scaffold for molecular sensing via surface-enhanced Raman scattering. J Phys Chem C. 2021;125:2502–10.
45. Chang H, Ko E, Kang H, Cha MG, Lee Y-S, Jeong DH. Synthesis of optically tunable bumpy silver nanoshells by changing the silica core size and their SERS activities. RSC Adv. 2017;7:40255–61.
46. Ajdari N, Vyas C, Bogan SL, Lwaleed BA, Cousins BG. Gold nanoparticle interactions in human blood: a model evaluation. Nanomed Nanotechnol Biol Med. 2017;13:1531–42.
47. Kim H-M, Jeong S, Hahm E, Kim J, Cha MG, Kim K-M, Kang H, Kyeong S, Pham X-H, Lee Y-S. Large scale synthesis of surface-enhanced Raman scattering nanoprobes with high reproducibility and long-term stability. J Ind Eng Chem. 2016;33:22–7.
48. Kang H, Jeong S, Park Y, Yim J, Jun B-H, Kyeong S, Yang J-K, Kim G, Hong S, Lee LP, et al. Near-infrared SERS nanoprobes with plasmonic Au/Ag hollow-shell assemblies for in vivo multiplex detection. Adv Funct Mater. 2013;23:3719–27.

Publisher's Note
Springer Nature remains neutral with regard to jurisdictional claims in published maps and institutional affiliations.